Non-Dicke decay in a small spherical sample with radially varying density

Richard Friedberg
Department of Physics, Columbia University, New York, New York 10027, USA

Jamal T. Manassah*
Department of Electrical Engineering, City College of New York, New York, New York 10031, USA

(Received 28 September 2011; published 23 January 2012)

It is a familiar fact that, in an isolated sphere or ellipsoid of uniform polarization density, the electrostatic field also is uniform. Because of this, the state of uniform polarization in a spherical sample of uniformly distributed two-level atoms is an eigenmode of the coherent decay process in the limit of a small radius compared to the resonant wavelength of a single atom. Consequently, in this special geometry, the Dicke picture of uniform exponential decay should hold. In nonspheroidal geometries or in spherical geometries with nonuniform atomic density, the decay should be more complicated. Here, we find the characteristic equations that determine the eigenmodes of the Lienard-Wiechert interaction for a partly hollowed sphere of identical two-level atoms in two different radial configurations. We show that the Dicke picture for emission from a coherently prepared sample does not correctly describe the system's dynamics even when we take the radius of the sphere to be much smaller than the radiation wavelength.

DOI: 10.1103/PhysRevA.85.013834 PACS number(s): 42.50.Nn

I. INTRODUCTION

We consider the coherent radiative emission [1–6] from a cloud of N identical two-level atoms. The Dicke picture for a small cloud (dimension $\ll$ resonant wavelength) envisions that, if the state is initially symmetric in all the atoms, it will remain so throughout the decay. Here, we mainly consider the case that the initial state is one of weak excitation. This problem is linear in the amplitude of the excited state, and in the Dicke picture, the decay is purely exponential, with a rate N times that of the isolated atom.

This picture was called into question [7] on the ground that the interaction energy,

$$W_{a\,b} = \exp(ikr_{ab})\left[\frac{\vec{p}_a \circ \vec{p}_b^{\,*} - 3\vec{p}_a \circ \hat{r}_{ab}\, p_b^{*} \circ \hat{r}_{ab}}{r_{ab}^3}(1-ikr_{ab}) - \frac{k^2}{r_{ab}}(\vec{p}_a \circ \vec{p}_b^{\,*} - \vec{p}_a \circ \hat{r}_{ab}\, \vec{p}_b^{\,*} \circ \hat{r}_{ab})\right], \tag{1.1}$$

between two dipoles $\vec{p}_a, \vec{p}_b$ at separation $\vec{r}_{ab} = r_{ab}\hat{r}_{ab}$ oscillating synchronously at frequency $\omega = kc$ becomes, at a short distance ($kr_{ab} \ll 1$),

$$W_{ab} = \frac{\vec{p}_a \circ \vec{p}_b^{\,*} - 3\vec{p}_a \circ \hat{r}_{ab}\vec{p}_b^{\,*} \circ \hat{r}_{ab}}{r_{ab}^3} - \frac{k^2(\vec{p}_a \circ \vec{p}_b^{\,*} + \vec{p}_a \circ \hat{r}_{ab}\vec{p}_b^{\,*} \circ \hat{r}_{ab})}{2r_{ab}} - \frac{2}{3}ik^3\,\vec{p}_a \circ \vec{p}_b^{\,*}, \tag{1.2}$$

whose real part $O(1/r_{12}^3)$ induces frequency shifts much larger than the radiation rate $O(k^3)$ given by the imaginary part. Since, even in the small sample, the frequency shift induced in a particular atom, in general, would depend strongly on the position of the atom within the sample, it was argued that the parts of the sample would dephase quickly before the radiation had time to occur significantly.

But in a uniformly dense sphere with initially uniform polarization [8], the resulting field also is uniform in the limit $kR \to 0$, and the sample does not dephase. (See also Ref. [9], Sec. II; Ref. [10], Sec. VIII. R is the radius of the sphere, and $2\pi/k$ is the resonant wavelength.) Thus, Dicke decay should take place in the uniform small sphere but not in one of variable density.

In this paper, we will consider a small spherical sample with either a uniformly filled shell and a central hollow or a shell and a central core both uniformly filled with the same density and separated by a gap. (The shell-plus-core case, with the initial excitation uniform, must not be confused with that of Ref. [9], Sec. VII in which the atomic density is uniform but the initial excitation is not.) We will treat these two configurations by means of the full Maxwell equations for the field and find numerical results for a small but finite sphere ($kR = 0.05$). These calculations involve the inversion of a matrix containing spherical Bessel functions of both j_1 and n_1 types, whose ratio is $O[(kR)^{-3}]$. The numerical results become unreliable when this ratio exceeds $\approx 10^5$. Hence, one cannot go with desired accuracy below $kR \approx 10^{-2}$ using the present algorithm. In the appendix, we will illustrate how one can obtain, through a double-series expansion of the eigenmode characteristic determinant, analytic results for the cooperative frequency shift and the cooperative decay rate that are exact in the limit $kR \to 0$.

In Sec. II, we recall the fundamental equations governing the dynamics of the system and present the formulas for the fields $\vec{\mathbf{E}}$ and $\vec{\mathbf{B}}$ within a region of uniform density in a general eigenmode of a spherically symmetric sample of any size. In Sec. III, we specialize for dipole ($l = 1$) symmetry and find the boundary conditions that determine eigenvalues and eigenfunctions in the shell-plus-hollow configuration. In Secs. IV and V, we do the same for the shell-plus-core configuration. In each configuration, we find that a small number of modes (two and three, respectively) dominate the short-time dynamics when $kR \ll 1$. These modes have wavelength $\gg 2\pi/k$. Other modes have short wavelength ($< R$) and do not enter appreciably for $kR = 0.05$. Non-Dicke behavior is found for this value of kR. We conclude in Sec. VI.

*jmanassah@gmail.com

II. FUNDAMENTAL EQUATIONS

One may consider the complex energy given by Eq. (1.1) as inducing a time development in accordance with quantum mechanics. This leads eventually to two equations [see Eqs. (2.4) and (2.5) of Ref. [10], note, however, that here we are using cgs units, i.e., $\varepsilon_0 \to 1/(4\pi)$],

$$\vec{\mathbf{P}}(\vec{r}) = -\frac{n\wp^2}{\hbar(\omega-\omega_0)}\vec{\mathbf{E}}_L(\vec{r}) = \frac{n\wp^2}{\hbar(\omega-\omega_0+\omega_L)}\vec{\mathbf{E}}(\vec{r}), \tag{2.1}$$

$$\vec{\mathbf{E}}_L(\vec{r}) = \vec{\mathbf{E}}(\vec{r}) + \frac{4}{3}\pi\vec{\mathbf{P}}(\vec{r}) = -\int d^3\vec{r}'\exp(ik\Re)\left[\left(\frac{1}{\Re^3} - i\frac{k}{\Re^2}\right)[\vec{\mathbf{P}}(\vec{r}') - 3\hat{\Re}\hat{\Re}\circ\vec{\mathbf{P}}(\vec{r}')] - \frac{k^2}{\Re}[\vec{\mathbf{P}}(\vec{r}') - \hat{\Re}\hat{\Re}\circ\vec{\mathbf{P}}(\vec{r}')]\right], \tag{2.2}$$

where $\vec{\mathbf{E}}_L$ is the local electric field, $\vec{\Re} = \Re,\hat{\Re} = \vec{r} - r'$, $\wp$ is the electric dipole matrix element, and $\omega_L$is the Lorentz shift $= \frac{1}{3}\frac{4\pi n\wp^2}{\hbar}$ arising from the term $\frac{4}{3}\pi\vec{\mathbf{P}}$ in Eq. (2.2).

In Eqs. (2.1) and (2.2), it has been assumed that the polarization density $\vec{\mathbf{P}}(\vec{r})$ and the Maxwell and local electric fields have a common time dependence $\exp(-i\omega t)$ and that sums over atoms may be replaced by integrals over space. Equation (2.1) holds only in the occupied regions where the number density is n. In the empty regions, $\vec{\mathbf{P}} = 0$. Equation (2.2) holds in all space, although the integral over $\vec{r}'$ can be regarded as limited to the occupied region since $\vec{\mathbf{P}}(\vec{r}')$ vanishes elsewhere.

Equations (2.1)–(2.2) describe an eigenmode of the linearized Maxwell-Bloch system pertaining to a sample of atoms weakly excited. We will take the frequency ω to be

$$\omega = \omega_0 - \omega_L - i\lambda, \tag{2.3}$$

so that Re(λ) represents decay of magnitude and Im(λ) represents a frequency shift that varies from mode to mode. Note that, in Ref. [10], we defined λ by $\omega = \omega_0 - i\lambda$ so that λ in that paper corresponds to $\lambda - i\omega_L$ in the present notation. Strictly, the quantity $k = \omega/c$ on the right-hand side of Eq. (2.2) should vary slightly from mode to mode in accordance with Eq. (2.3), but we neglect this variation and replace k by $k_0 = \omega_0/c$ for all modes. Thus, Eqs. (2.1) and (2.2) become

$$\vec{\mathbf{P}}(\vec{r}) = -\frac{n\wp^2}{\hbar\lambda}\vec{\mathbf{E}} \quad \text{(occupied region)}, \tag{2.4}$$

and

$$\vec{\mathbf{E}}(\vec{r}) + \frac{4}{3}\pi\vec{\mathbf{P}}(\vec{r}) = -\int d^3\vec{r}'\exp(ik_0\Re)\left[\left(\frac{1}{\Re^3} - i\frac{k_0}{\Re^2}\right)[\vec{\mathbf{P}}(\vec{r}') - 3\hat{\Re}\hat{\Re}\circ\vec{\mathbf{P}}(\vec{r}')] - \frac{k_0^2}{\Re}[\vec{\mathbf{P}}(\vec{r}') - \hat{\Re}\hat{\Re}\circ\vec{\mathbf{P}}(\vec{r}')]\right]. \tag{2.5}$$

Suitable treatment of Eq. (2.5) shows that the Maxwell fields $\vec{\mathbf{E}}$ and $\vec{\mathbf{B}}$ satisfy

$$\left(\nabla^2 + k_0^2\right)\vec{\mathbf{E}} = 0, \quad \left(\nabla^2 + k_0^2\right)\vec{\mathbf{B}} = 0, \tag{2.6}$$

in the empty region, but

$$(\nabla^2 + k'^2)\vec{\mathbf{E}} = 0, \quad (\nabla^2 + k'^2)\vec{\mathbf{B}} = 0, \tag{2.7}$$

in the occupied region, where

$$k'^2\vec{\mathbf{E}} = k_0^2(\vec{\mathbf{E}} + 4\pi\vec{\mathbf{P}}), \tag{2.8a}$$

or, equivalently,

$$\frac{k'^2}{k_0^2} = 1 + \frac{4\pi n\wp^2}{i\hbar\lambda}. \tag{2.8b}$$

The fields $\vec{\mathbf{E}}$ and $\vec{\mathbf{B}}$ also are related by

$$\vec{\nabla}\times\vec{\mathbf{E}} = i\,k_0\,\vec{\mathbf{B}}, \tag{2.9a}$$

$$\vec{\nabla}\times\vec{\mathbf{B}} = -i\,k_0(\vec{\mathbf{E}} + 4\pi\vec{\mathbf{P}}) = -i\frac{k'^2}{k_0}\vec{\mathbf{E}}, \tag{2.9b}$$

so that the tangential components of $\vec{\mathbf{E}}$ and $\vec{\mathbf{B}}$ are continuous across boundaries. (See Ref. [10] for more details.)

From Eq. (2.8), we find that λ for any mode is given by

$$\lambda = i\,\frac{C\,k_0^2}{k_0^2 - k'^2}, \tag{2.10}$$

where $C = 4\pi\wp^2 n/\hbar$. (Note that k' is complex and different for each mode.)

In a spherical geometry, the possible solutions of Eq. (2.7) are designated by angular indices l,m, and a radial index s as well as a binary choice (E,M) [10,11]. Since our initial condition is one of uniform polarization, we need consider only electric dipole modes (E) with $l = 1$ and $m = 0$ and, henceforth, suppress the angular indices. Then, the solution

for an eigenmode (s), in region L, has the form

$$\vec{\mathbf{B}}(x,\theta,\phi) = [a_1 j_1(v_s x) + a_2 n_1(v_s x)]\, P_l^1[\cos(\theta)]\,\hat{e}_\phi, \tag{2.11}$$

$$\begin{aligned}\vec{\mathbf{E}}(x,\theta,\phi) = -\frac{iu}{v_s^2 x}\big(&2[a_1 j_1(v_s x) + a_2 n_1(v_s x)]P_1[\cos(\theta)]\hat{e}_r \\ &+ \{a_1[(v_s x)j_0(v_s x) - j_1(v_s x)] + a_2[(v_s x)n_0(v_s x) \\ &- n_1(v_s x)]\}P_1^1[\cos(\theta)]\hat{e}_\theta\big),\end{aligned} \tag{2.12}$$

in an occupied region and a similar expression with $v_s \to u$ in an empty region. The dimensionless quantities x, v_s, and u are defined as $x = r/R, v_s = k_s R$, and $u = k_0 R$. j_1, n_1, and $h_1^{(1)} = j_1 + i n_1$ are the spherical Bessel functions of order 1; j_0, n_0, h_0 those of order 0; and P_1, P_1^1 are Legendre polynomials.

The normalized eigenvalues $\Lambda_s = \lambda_s/C$ for the different modes then are given by

$$\Lambda_s = i\frac{u^2}{u^2 - v_s^2}. \tag{2.13}$$

An additional term $-i/3$ would be added to Eq. (2.10) if we were to define λ as in Ref. [10] including the effect of the local-field correction.

III. EXACT EIGENVECTORS AND EIGENVALUES FOR THE SHELL-PLUS-HOLLOW CONFIGURATION

The density of the resonant atoms in this configuration is given by

$$\begin{aligned} n &= 0, \quad 0 \leqslant r \leqslant \beta R, \\ n &\neq 0, \quad \beta R < r \leqslant R, \\ n &= 0, \quad r > R. \end{aligned}$$

The magnetic flux density in the different regions is given by

$$\begin{aligned} \mathbf{B}_\phi &= C_1 j_1(ux), \quad 0 \leqslant r \leqslant \beta R, \\ \mathbf{B}_\phi &= B_1 j_1(v_s x) + B_2 n_1(v_s x), \quad \beta R < r \leqslant R, \\ \mathbf{B}_\phi &= A_2 h_1^{(1)}(ux), \quad r > R. \end{aligned} \tag{3.1}$$

The continuity of $\mathbf{B}_\phi$ at $x = \beta$ and $x = 1$ (we assume the atoms have no internal magnetization) gives the equations,

$$C_1 j_1(u\beta) = B_1 j_1(v_s\beta) + B_2 n_1(v_s\beta), \tag{3.2}$$

$$B_1 j_1(v_s) + B_2 n_1(v_s) = A_2 h_1^{(1)}(u). \tag{3.3}$$

The continuity of $\mathbf{E}_\theta$ at $x = \beta$ and $x = 1$ gives the equations,

$$C_1 v_s^2[u\beta j_0(\beta u) - j_1(\beta u)] = B_1 u^2[v_s\beta j_0(\beta v_s) - j_1(\beta v_s)] + B_2 u^2[v_s\beta n_0(\beta v_s) - n_1(\beta v_s)], \tag{3.4}$$

$$B_1 u^2[v_s j_0(v_s) - j_1(v_s)] + B_2 u^2[v_s n_0(v_s) - n_1(v_s)] = A_2 v_s^2\big[u h_0^{(1)}(u) - h_1^{(1)}(u)\big]. \tag{3.5}$$

(See Refs. [10,11] for details.)

The characteristic equation for $v_s$is obtained by imposing the condition that the linear system [Eqs. (3.2)–(3.5)] has solutions, i.e.,det($\mathbf{M}$) = 0, where $\mathbf{M}$ is given by

$$\begin{pmatrix} j_1(u\beta) & -j_1(v_s\beta) & -n_1(v_s\beta) & 0 \\ v_s^2[u\beta j_0(\beta u) - j_1(\beta u)] & -u^2[v_s\beta j_0(\beta v_s) - j_1(\beta v_s)] & -u^2[v_s\beta n_0(\beta v_s) - n_1(\beta v_s)] & 0 \\ 0 & j_1(v_s) & n_1(v_s) & -h_1^{(1)}(u) \\ 0 & u^2[v_s j_0(v_s) - j_1(v_s)] & u^2[v_s n_0(v_s) - n_1(v_s)] & -v_s^2\big[u h_0^{(1)}(u) - h_1^{(1)}(u)\big] \end{pmatrix}. \tag{3.6}$$

In our numerical search for the roots of Eq. (3.6), we select the two roots with $\mathrm{Im}(v_s) < 0$ and $\mathrm{Re}(v_s) > 0$ closest to 0.

In Fig. 1, we plot the real and imaginary parts of the dominant v_s's for a sphere with a small radius ($u = 0.05$) as a function of β and, in Fig. 2, the corresponding values of the normalized eigenvalues $\Lambda_s = \lambda_s/C$. We note that:

(1) For $\beta \ll 1$ and $s = 2$, Fig. 1 gives $\mathrm{Re}(v_2) \to 0$ and Fig. 2 gives $\lambda_2 \to \lambda_D + \frac{1}{3}iC$ as in the completely filled small sphere. In this limit, the nonzero value of $\mathrm{Im}(v_2)$ is due to the fact that our numerical value of $k_0 R$ differs from zero.

(2) The sum $\lambda_1 + \lambda_2$ is equal numerically to $\lambda_D + iC$ for all β. [The Dicke decay rate λ_D is defined by $\lambda_D = N\gamma_1/2 = nV(\frac{2}{3}\wp^2 k_0^3/\hbar)$, where V is the active volume $\frac{4}{3}\pi R^3(1-\beta^3)$. Since the normalized quantity shown in Fig. 2(a) is $\Lambda_D = \lambda_D/C$, where $C = (4\pi n\wp^2/\hbar)$, Λ_D is proportional to $(1-\beta^3)$ as shown.] The sum rule $\sum_s \mathrm{Re}(\lambda_s) = \lambda_D$ is exact for any atomic distribution on account of a trace argument. In the limit $k_0 R \to 0$, this sum rule would include only the two modes shown. For our sample ($k_0 R = 0.05$), the contribution of other (short-wavelength) modes turns out to be less than 1/1000 of the total. We find numerically that the small quantity $\lambda_D - \mathrm{Re}(\lambda_1) - \mathrm{Re}(\lambda_2)$ is positive as required. The numerical finding that $\mathrm{Im}(\Lambda_1) + \mathrm{Im}(\Lambda_2) = 1$ also is exact for $k_0 R = 0$.

(3) The quantities $B_1/C_1, B_2/C_1$, and A_2/C_1 are obtained by solving

$$\begin{pmatrix} j_1(v_s\beta) & n_1(v_s\beta) & 0 \\ j_1(v_s) & n_1(v_s) & -h_1^{(1)}(u) \\ u^2[v_s j_0(v_s) - j_1(v)] & u^2[v_s n_0(v_s) - n_1(v_s)] & -v_s^2\left[uh_0^{(1)}(u) - h_1^{(1)}(u)\right] \end{pmatrix} \begin{pmatrix} B_1/C_1 \\ B_2/C_1 \\ A_2/C_1 \end{pmatrix} = \begin{pmatrix} j_1(u\beta) \\ 0 \\ 0 \end{pmatrix}, \tag{3.7}$$

and the electric-field components in the resonant medium are given by

$$\mathbf{E}_r^{(s)} = -\frac{2iu}{v_s^2 x}\left[\left(\frac{B_1}{C_1} j_1(v_s x) + \frac{B_2}{C_1} n_1(v_s x)\right)\right], \tag{3.8}$$

$$\mathbf{E}_\theta^{(s)} = -\frac{iu}{v_s^2 x}\left(\frac{B_1}{C_1}\left[(v_s x)\, j_0(v_s x) - j_1(v_s x)\right] + \frac{B_2}{C_1}\left[(v_s x)\, n_0(v_s x) - n_1(v_s x)\right]\right). \tag{3.9}$$

In Fig. 3, we plot the components of the electric field in each mode as a function of space for the same value of $k_0 R$ as in Figs. 1 and 2 and for $\beta = 0.5$. We note that the value of the field is not constant as it would be for the completely filled sphere.

IV. EXACT EIGENFREQUENCIES FOR THE SHELL-PLUS-CORE CONFIGURATION

In this configuration, the resonant atoms have a single constant density throughout two filled regions.

(II) $\beta R \leqslant r \leqslant R$ shell,

(IV) $r < \gamma R$ core,

where $1 > \beta > \gamma > 0$. The two regions

(I) $r > R$,

(III) $\beta R > r > \gamma$ gap

contain vacuums.

The atomic density, thus, is

$$\rho = \begin{cases} n, & \text{in II and IV,} \\ 0, & \text{in I and III.} \end{cases} \tag{4.1}$$

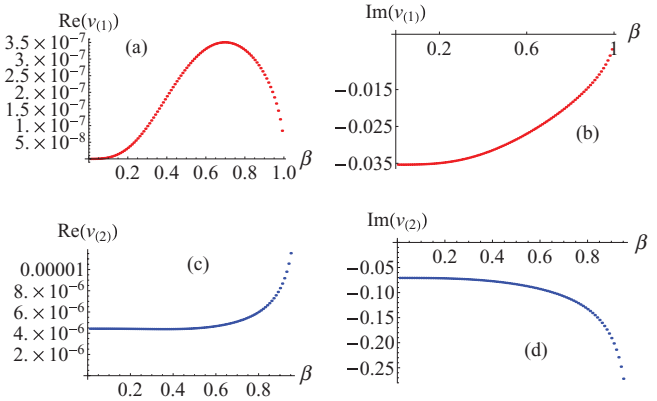

FIG. 1. (Color online) For the shell-plus-hollow configuration, the real and imaginary parts of the eigenmode wave vectors as a function of β. $u = 0.05$. (a) and (b) $s = 1$; (c) and (d) $s = 2$.

And so, we have $(\nabla^2 + k_0^2)\vec{\mathbf{B}} = 0$ in regions I and III and $(\nabla^2 + k_s^2)\vec{\mathbf{B}} = 0$ in regions II and IV.

For the electric modes with $l = 1$ and $m = 0$, we have $\vec{\mathbf{B}} = \mathbf{B}_\phi P_1^1(\cos\theta)\,\hat{\mathbf{e}}_\phi = \mathbf{B}_\phi(-\sin\theta)\hat{e}_\phi$ [10], where

$$\mathbf{B}_\phi = \begin{cases} A_2\, h_1^{(1)}(ux) & \text{I} \\ B_1 j_1(v_s x) + B_2 n_1(v_s x) & \text{II} \\ C_1 j_1(ux) + C_2 n_1(ux) & \text{III} \\ D_1 j_1(v_s x) & \text{IV} \end{cases} \tag{4.2}$$

Note that v_s has the same value in regions II and IV since the density is the same.

Continuity of $\mathbf{B}_\phi$ at the interfaces I-II, II-III, and III-IV gives the relations [11],

$$B_1 j_1(v_s) + B_2 n_1(v_s) = A_2 h_1^{(1)}(u), \tag{4.3}$$

$$C_1 j_1(u\beta) + C_2 n_1(u\beta) = B_1 j_1(v_s\beta) + B_2 n_1(v_s\beta), \tag{4.4}$$

$$D_1 j_1(v_s\gamma) = C_1 j_1(u\gamma) + C_2 n_1(u\gamma). \tag{4.5}$$

The continuity of the tangential component of the electric field at each of the interfaces gives the relations,

$$B_1 u^2[v_s j_0(v_s) - j_1(v_s)] + B_2 u^2[v_s n_0(v_s) - n_1(v_s)] = A_2 v_s^2\left[uh_1^{(1)}(u) - h_0^{(1)}(u)\right], \tag{4.6}$$

$$C_1 v_s^2[u\beta j_0(\beta u) - j_1(\beta u)] + C_2 v_s^2[u\beta n_0(\beta u) - n_1(\beta u)] = B_1 u^2[v_s\beta j_0(\beta v_s) - j_1(\beta v_s)] + B_2 u^2[v_s n_0(\beta v_s) - n_1(\beta v_s)], \tag{4.7}$$

$$D_1 u^2[v_s\gamma j_0(\gamma v_s) - j_1(\gamma v_s)] = C_1 v_s^2[u\gamma j_0(\gamma u) - j_1(\gamma u)] + C_2 v_s^2[u\gamma n_0(\gamma u) - n_1(\gamma u)]. \tag{4.8}$$

Equations (4.3)–(4.8) form a system of six homogeneous linear equations for the unknowns $\{A_2, B_1, B_2, C_1, C_2, D_1\}$. The existence of a solution requires that the determinant of the matrix describing the above system be zero. The characteristic

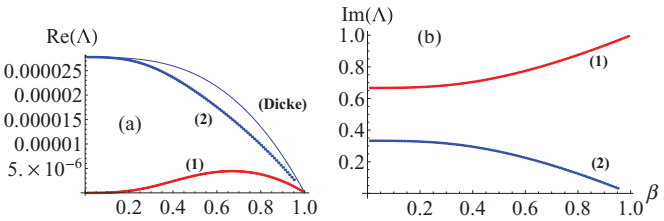

FIG. 2. (Color online) For the shell-plus-hollow configuration, (a) comparison of the value of the Dicke single-mode value for Re(Λ) with the corresponding values for the different leading modes as a function of β. (b) Comparison of the values of Im(Λ) for the different leading modes. $u = 0.05$.

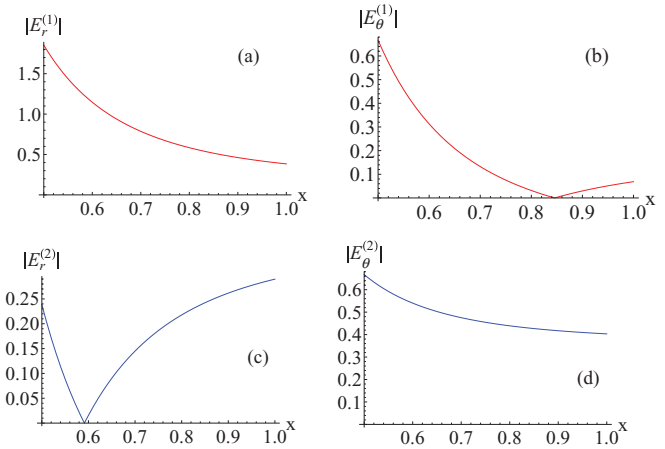

FIG. 3. (Color online) For the shell-plus-hollow configuration at fixed $\beta = 0.5$ and for $u = 0.05$, the radial component and the tangential component of the electrical field are plotted as a function of the normalized radial variable for each of the two leading modes. (a) and (b) $s = 1$; (c) and (d) $s = 2$.

complex wave vectors for this system are the roots of this equation. In our numerical search for the roots of the secular determinant, we select the three roots with $\mathrm{Im}(v) < 0$ and $\mathrm{Re}(v) > 0$ that are closest to zero. (We verify later that these eigenmodes form a complete basis for small values of u.)

In Fig. 4, we plot, as a function of β for fixed γ, the values of the leading wave vectors for a small value of u (=0.05). We note that the mode with $s = 2$ is the branch that in the limit $\beta \to \gamma$ goes to the $s = 1$ mode of the uniform sphere. [The indices here are assigned on the basis of the increasing value of $|\mathrm{Im}(v)|$ as shown in Figs. 4(b), 4(d), and 4(f).]

We define the dominant mode in coherent emission as that with the largest value of $\mathrm{Re}(\Lambda)$. To identify the dominant mode, in Fig. 5(a), we show the values of $\mathrm{Re}(\Lambda_s)$ for all three leading

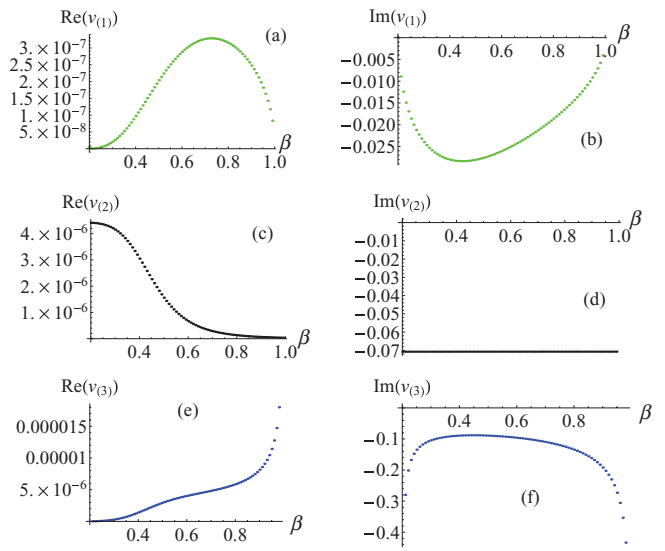

FIG. 4. (Color online) For shell-plus-core configuration, the real and imaginary parts of the eigenmode wave vectors as a function of β, the outer radius of the gap. $\gamma = 0.2$. $u = 0.05$. (a) and (b) $s = 1$; (c) and (d) $s = 2$; (e) and (f) $s = 3$.

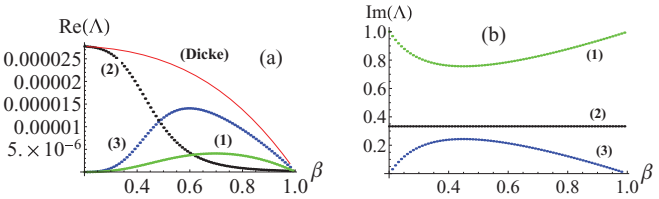

FIG. 5. (Color online) For shell-plus-core configuration, (a) comparison of the value of the Dicke single-mode value for $\mathrm{Re}(\Lambda)$ with the corresponding values for the different leading modes in the present model as a function of β. (b) Comparison of the values of $\mathrm{Im}(\Lambda)$ for the different leading modes. $u = 0.05$. $\gamma = 0.2$.

modes and compare them to that of the single mode of the Dicke model.

We note that, depending on the value of β, the dominant mode can be either the mode with $s = 2$ or the mode with $s = 3$. For $u = 0.05$, the crossing occurs, for $\gamma = 0.2$, at about $\beta = 0.48$; but it is not a true crossing in that the values of $\mathrm{Im}(\Lambda)$ do not cross there.

In Fig. 5(b), we compare the value of $\mathrm{Im}(\Lambda)$ for the different modes as a function of β. We note that $\mathrm{Im}(\Lambda_{(2)}) = 1/3$ for all β, whereas, everywhere, $\mathrm{Im}(\Lambda_{(1)} + \Lambda_{(3)}) = 1$.

V. THE ELECTRIC-FIELD EIGENMODES FOR THE SHELL-PLUS-CORE CONFIGURATION

We now examine the spatial variation in the electric field in each of the three leading modes. Having determined the values of the complex wave vectors, one obtains the

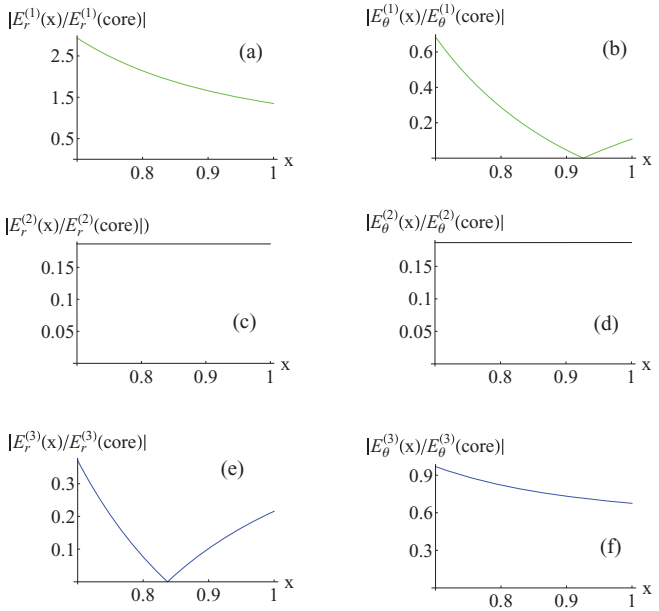

FIG. 6. (Color online) For shell-plus-core configuration at fixed $\gamma = 0.4$, $\beta = 0.7$, and for $u = 0.05$, the ratios of the radial component and of the tangential component of the electrical field in the outer shell to the corresponding components in the core are plotted against the normalized radial variable in the outer shell for each of the three leading modes. (a) and (b) $s = 1$; (c) and (d) $s = 2$; (e) and (f) $s = 3$.

ratios $(C_1/D_1, C_2/D_1, B_1/D_1, B_2/D_1, A_2/D_1)$ by solving the inhomogeneous system of equations,

$$\mathbf{M}\begin{bmatrix} C_1/D_1 \\ C_2/D_1 \\ B_1/D_1 \\ B_2/D_1 \\ A_2/D_1 \end{bmatrix} = \begin{bmatrix} j_1(v_s\alpha) \\ 0 \\ 0 \\ 0 \\ 0 \end{bmatrix}, \tag{5.1}$$

where

$$\begin{aligned}
&M_{13} = M_{14} = M_{15} = M_{25} = M_{35} = M_{41} \\
&\quad = M_{42} = M_{51} = M_{52} = 0, \\
&M_{11} = j_1(\gamma u), M_{12} = n_1(\gamma u), \\
&M_{21} = j_1(\beta u), \quad M_{22} = n_1(\beta u), \quad M_{23} = -j_1(\beta v_s), \\
&M_{24} = -n_1(\beta v_s), \\
&M_{31} = v_s^2\left[u\beta j_0(\beta u) - j_1(\beta u)\right], \\
&M_{32} = v_s^2\left[u\beta n_0(\beta u) - n_1(\beta u)\right], \\
&M_{33} = -u^2[v_s\beta j_0(\beta v_s) - j_1(\beta v)], \\
&M_{34} = -u^2[v_s\beta n_0(\beta v_s) - n_1(\beta v_s)], \\
&M_{43} = j_1(v_s), \quad M_{44} = n_1(v_s), \quad M_{45} = -h_1^{(1)}(u), \\
&M_{53} = u^2[v_s j_0(v_s) - j_1(v_s)], \quad M_{54} = u^2[v_s n_0(v_s) - n_1(v_s)], \\
&M_{55} = -v_s^2\left[uh_0^{(1)}(u) - h_1^{(1)}(u)\right].
\end{aligned}$$

The electric fields in the atomic medium (regions II and IV) associated with each of the eigenmodes are given by [10]

$$\begin{aligned}
\vec{\mathbf{E}}^{(s)} &= \mathbf{E}_r^{(s)} P_1[\cos(\theta)]\,\hat{e}_r + \mathbf{E}_\theta^{(s)} P_1^1[\cos(\theta)]\,\hat{e}_\theta \\
&= \mathbf{E}_r^{(s)}\cos(\theta)\,\hat{e}_r - \mathbf{E}_\theta^{(s)}\sin(\theta)\,\hat{e}_\theta,
\end{aligned} \tag{5.2}$$

where

$$\mathbf{E}_r^{(s)} = \begin{cases} -\frac{2iu}{v_s^2 x} j_1(v_s x) & \text{IV; } 0 \leqslant x \leqslant \gamma \\ -\frac{2iu}{v_s^2 x}\left[\left(\frac{B_1}{D_2} j_1(v_s x) + \frac{B_2}{D_2} n_1(v_s x)\right)\right] & \text{II; } \beta \leqslant x \leqslant 1 \end{cases}, \tag{5.3}$$

$$\mathbf{E}_\theta^{(s)} = \begin{cases} -\frac{iu}{v_s^2 x}[(v_s x) j_0(v_s x) - j_1(v_s x)] & \text{IV; } 0 \leqslant x \leqslant \gamma \\ -\frac{iu}{v_s^2 x}\left[\left(\frac{B_1}{D_2}[(v_s x) j_0(v_s x) - j_1(v_s x)] + \frac{B_2}{D_2}[(v_s x) n_0(v_s x) - n_1(v_s x)]\right)\right] & \text{II; } \beta \leqslant x \leqslant 1 \end{cases}. \tag{5.4}$$

As a check on our numerical algorithm, for $\gamma = 0.4$, $\beta = 0.7$, and $u = 0.05$, for each eigenmode $s = \{1,2,3\}$, we have verified that the magnetic flux density $\mathbf{B}_\phi$ obtained numerically is everywhere continuous.

In the Dicke model, the leading eigenmode should have $\vec{\mathbf{E}}$ constant throughout the atomic region. In our configuration, $\vec{\mathbf{E}}$ is necessarily nearly constant throughout the core (region IV) in each eigenmode but not necessarily throughout the outer shell (region II). In Fig. 6 we show, for each $s = \{1,2,3\}$, the variation with $x = r/R$, throughout the shell, of $\mathbf{E}_r$ and $\mathbf{E}_\theta$, normalized to their values in the core. We see indeed that $\vec{\mathbf{E}}$ nearly is constant throughout the shell in the $s = 2$ mode (but not in the others); its value in the shell, however, is only approximately 1/5 of its value in the core. In Fig. 7, for the $s = 2$ mode, for $\gamma = 0.2$, we plot the ratio of the magnitude of the field on the inner edge of the shell to its magnitude in the core as a function of β. Again, we establish that $\vec{\mathbf{E}}$ is, in general, far from uniform throughout the whole atomic region.

But how far is far? Let us take each $\vec{\mathbf{E}}_s$ to be normalized by $\int_{\text{II+IV}} |\mathbf{E}_s|^2\, d^3\vec{r} = 1$ [9] and the uniform initial $\vec{\mathbf{E}}_{\text{unif}}$ similarly normalized; then, if $\vec{\mathbf{E}}_{\text{unif}}$ is expressed as $\vec{\mathbf{E}}_{\text{unif}} = \sum_s I^{(s)}\vec{\mathbf{E}}_s$, the quantities $|I^{(s)}|^2$ can be regarded as probabilities that the system excited uniformly will behave according to the various eigenmodes. The coefficients $I^{(s)}$ are given by

$$I^{(s)} = \int_{\text{II+IV}} \vec{\mathbf{E}}_s \circ \vec{\mathbf{E}}_{\text{unif}}\, d^3\vec{r} = \frac{\int_{\text{II+IV}} \vec{\mathbf{E}}_s \circ \vec{\mathbf{E}}_{\text{unif}}\, d^3\vec{r}}{\sqrt{\int_{\text{II+IV}} |\mathbf{E}_s|^2 d^3\vec{r}}\sqrt{\int_{\text{II+IV}} |\mathbf{E}_{\text{unif}}|^2 d^3\vec{r}}}. \tag{5.5}$$

In terms of the un-normalized components (5.3) and (5.4),

$$|I^{(s)}| = \frac{\left|\int_0^\gamma \left(\frac{2}{3}\mathbf{E}_r^{(s)} + \frac{4}{3}\mathbf{E}_\theta^{(s)}\right)x^2 dx + \int_\beta^1 \left(\frac{2}{3}\mathbf{E}_r^{(s)} + \frac{4}{3}\mathbf{E}_\theta^{(s)}\right)x^2 dx\right|}{\left\{\left[\int_0^\gamma \left(\frac{2}{3}\left|\mathbf{E}_r^{(s)}\right|^2 + \frac{4}{3}\left|\mathbf{E}_\theta^{(s)}\right|^2\right)x^2 dx + \int_\beta^1 \left(\frac{2}{3}\left|\mathbf{E}_r^{(s)}\right|^2 + \frac{4}{3}\left|\mathbf{E}_\theta^{(s)}\right|^2\right)x^2 dx\right]\frac{2}{3}\left(1 + \gamma^3 - \beta^3\right)\right\}^{1/2}}. \tag{5.6}$$

In Table I, we give the values of $\{|I^{(s)}|\}$ for some selected values of $\{\beta,\gamma\}$. In the last column, for each configuration of $\beta$and γ, we give the value of $\sum_{s=1}^3 |I^{(s)}|^2$. We note that this sum is equal to 1 with an accuracy of better than 1/10 000, indicating that, for all practical purposes, these three modes form a complete basis for describing the quantum dynamics of emission for a hollowed sphere with this configuration for a small value of u. A similar check (not shown) has been performed for the two modes of the shell-plus-hollow configuration.

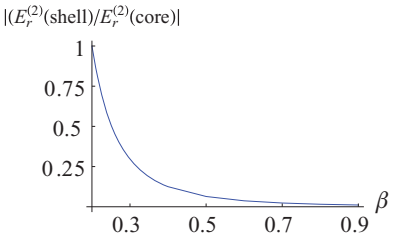

FIG. 7. (Color online) For shell-plus-core configuration at fixed $\gamma = 0.2$ and for $u = 0.05$, the ratio of the magnitude of the $s = 2$ mode electric-field radial component on the inner edge of the shell to its magnitude in the core is plotted as a function of β.

Furthermore, we note that, in general, no one mode has $|I^{(s)}|^2$ close to 1. Thus, the radiation during a time $O(\lambda_{\text{Dicke}}^{-1})$ will have significant contributions from all three modes, all with relative frequency shifts $\gg \lambda_{\text{Dicke}}$.

VI. CONCLUSION

We have carried out a study of coherent emission from a hollowed sphere in two configurations, using a full Maxwell treatment yielding equations and boundary conditions valid for any size sphere. For numerical work, we have specialized, for a very small sphere, $k_0 R = 0.05$. Our results verify the prediction [8] that, although the simple Dicke model [1] holds well for a small sphere of uniform density, it should not be valid, even when the sample is small for general shapes or (even with spherical symmetry) for general density distributions. In such a sample, the position dependence of large frequency shifts [7] distorts the Dicke picture in a time much shorter than the decay time.

We have found that the dynamics of the system is dominated, at times not much longer than the Dicke decay time, by only two modes in the hollow-shell configuration, or by three in the core-plus-shell configuration. These modes have wavelength much larger than that of the resonant light. All other modes have wavelength smaller than the sample size and are found to contribute negligibly to the initial state of uniform polarization. The beats among the few dominant modes are sufficient to produce the distortion of Dicke decay, which can alternatively be understood [7] as due to position-dependent frequency shifts.

TABLE I. For the shell-plus-core-filled configuration: Magnitude of the projection of the electric field of eigenmode (s) over the uniform state in the direction $\hat{e}_z$.

	$\gamma = 0.2$			
β	$\lvert I^{(1)}\rvert$	$\lvert I^{(2)}\rvert$	$\lvert I^{(3)}\rvert$	$\sum_{s=1}^{3} \lvert I^{(s)}\rvert$
0.4	0.219 983	0.855 170	0.469 353	0.999 999
0.5	0.328 814	0.632 564	0.701 245	0.999 999
0.6	0.411 556	0.436 746	0.799 921	0.999 999
0.7	0.470 782	0.312 841	0.824 922	1.000 000
0.8	0.512 680	0.246 233	0.822 514	1.000 000
0.9	0.540 765	0.231 825	0.808 598	1.000 000

The calculations in this paper also apply, with slight modifications, to super-radiance from a nearly inverted state in which the initial fraction of atoms in the ground state is small, but their number is sufficient to support a coherent polarization density. The eigenfunctions and eigenvalues are the same as calculated here, but the time development of each mode follows $\exp(\lambda t)$ instead of $\exp(-\lambda t)$. (The Lorentz shift is also reversed [12,13].)

The long-time behavior of the inverted system differs significantly from that of the weakly excited system. In the latter system, the dominant modes studied here die out exponentially at different rates, and the weakest of these modes [having the smallest $\text{Re}(\lambda)$] will persist the longest, giving rise to a period of genuine exponential decay but with a decay rate considerably less than λ_D. Eventually, this decay will progress so far that the nondominant (short-wavelength) modes ignored in our calculation will be all that will be left; they will produce a residual incoherent radiation of much longer duration.

In the inverted system, the incoherent radiation produced by the nondominant modes would characterize the preinitial period of spontaneous radiation and quantum fluctuations studied in Ref. [14]. In describing our nearly inverted initial state, we assume that any such period already has passed before time $t = 0$. The dominant modes then grow differentially so that the strongest mode [largest $\text{Re}(\lambda)$] presently prevails and the growth becomes exponential but still is slower than the Dicke rate. Finally, nonlinearity sets in when the fraction of ground-state atoms is no longer small, and the present analysis no longer holds. This situation also has been described for a large sphere of uniform density [15].

An interesting situation arises in the nearly inverted case when the two strongest modes have nearly the same $\text{Re}\,(\lambda)$; then, the beats between them [16], observable on the fast time scale $O\,(1/C)$, continue for a time much longer than λ_D. A similar phenomenon occurs in the weakly excited case, when the two weakest dominant modes nearly are degenerate in $\text{Re}\,(\lambda)$. [Note that a crossing in $\text{Re}\,(\lambda)$ is not accompanied by one in $\text{Im}\,(\lambda)$.]

APPENDIX

In this Appendix, we give the analytic expressions for both the shift and the width for the shell plus hollow configuration as a function of the parameter β for $k_0 R \to 0$, and compare these expressions with the numerically obtained results.

We write the solvability condition for this configuration, i.e., Eq. (3.6), as a power series in v and in u, i.e., all terms in this expansion are of the form $v^m u^n$. We include all terms such that $\max\,(m) = 4$ and $\max\,(m + n) = 7$. This truncated series reduces to the following quadratic equation in v^2:

$$c + bv^2 + av^4 = 0, \tag{A1}$$

where

$$c = 2(-1+\beta^3)u^4 + \tfrac{1}{5}(-5+\beta^2+5\beta^3-\beta^5)u^6 + i\tfrac{2}{3}(-1+\beta^3)u^7, \tag{A2}$$

$$b = (-5-4\beta^3)u^2 + \tfrac{1}{10}(-11+19\beta^2-10\beta^3+2\beta^5)u^4 + i\tfrac{2}{3}(-1+\beta^3)u^5, \tag{A3}$$

$$a = 2(-1+\beta^3) + \tfrac{1}{10}(19-11\beta^2-10\beta^3+2\beta^5)u^2 - i\tfrac{4}{3}(-1+\beta^3)u^3. \tag{A4}$$

Writing the solutions of v^2 to fifth order in u gives

$$v_1^2 = \frac{(5+4\beta^3-3\sqrt{1+8\beta^3})}{4(-1+\beta^3)}u^2 + \frac{1}{240}\Bigg[-\frac{3(-19-19\beta-8\beta^2+2\beta^3+2\beta^4)(5+4\beta^3-3\sqrt{1+8\beta^2})}{(-1+\beta)(1+\beta+\beta^2)^2} + \frac{2\Big(33-57\beta^2+30\beta^3-6\beta^5+\frac{-91+131\beta^2-58\beta^3+50\beta^5-40\beta^6+8\beta^8}{\sqrt{1+8\beta^3}}\Big)}{(-1+\beta^3)}\Bigg]u^4 + i\frac{\Big[2-\frac{2}{\sqrt{1+8\beta^3}}+\beta^3\Big(1-\frac{7}{1+8\beta^3}\Big)\Big]}{2-2\beta^3}u^5 + O(u^6), \tag{A5}$$

$$v_2^2 = \frac{(5+4\beta^3+3\sqrt{1+8\beta^3})}{4(-1+\beta^3)}u^2 + \frac{1}{240}\Bigg(-\frac{3(-19-19\beta-8\beta^2+2\beta^4)(5+4\beta^3+3\sqrt{1+8\beta^2})}{(-1+\beta)(1+\beta+\beta^2)^2} + \frac{2\Big(33-57\beta^2+30\beta^3-6\beta^5+\frac{91-131\beta^2+58\beta^3-50\beta^5+40\beta^6-8\beta^8}{\sqrt{1+8\beta^3}}\Big)}{(-1+\beta^3)}\Bigg)u^4 + i\frac{\Big[2+\frac{2}{\sqrt{1+8\beta^3}}+\beta^3\Big(1+\frac{7}{1+8\beta^3}\Big)\Big]}{2-2\beta^3}u^5 + O(u^6). \tag{A6}$$

Recalling that $\Lambda = i\frac{u^2}{u^2-v^2}$, these, for third order in u, are given by

$$\Lambda_1 = i\frac{4(-1+\beta^3)}{3(-3+\sqrt{1+8\beta^3})} - i\frac{8(-1+\beta^3)^2}{9(-3+\sqrt{1+8\beta^3})^2}\Bigg(-\frac{(19+19\beta+8\beta^2-2\beta^3-2\beta^4)(378\,000+302\,400\beta^3-226\,800\sqrt{1+8\beta^3})}{3024000(-1+\beta)(1+\beta+\beta^2)^2} - \frac{83\,160-143\,640\beta^2+75\,600\beta^3-15\,120\beta^5+\frac{2520(-91+131\beta^2-58\beta^3+50\beta^5-40\beta^6+8\beta^8)}{\sqrt{1+8\beta^3}}}{-151\,200+151\,200\beta^3}\Bigg)u^2 - \frac{8[(-1+\beta^3)(-2-7\beta^3+(2+\beta^3)\sqrt{1+8\beta^3})]}{9[\sqrt{1+8\beta^3}(-3+\sqrt{1+8\beta^3})^2]}u^3, \tag{A7}$$

$$\Lambda_2 = -i\frac{4(-1+\beta^3)}{3(+3+\sqrt{1+8\beta^3})} - i\frac{8(-1+\beta^3)^2}{9(+3+\sqrt{1+8\beta^3})^2}\Bigg(-\frac{(19+19\beta+8\beta^2-2\beta^3-2\beta^4)(378\,000+302\,400\beta^3+226\,800\sqrt{1+8\beta^3})}{3024\,000(-1+\beta)(1+\beta+\beta^2)^2} - \frac{83160-143640\beta^2+75600\beta^3-15120\beta^5-\frac{2520(-91+131\beta^2-58\beta^3+50\beta^5-40\beta^6+8\beta^8)}{\sqrt{1+8\beta^3}}}{-151200+151200\beta^3}\Bigg)u^2 - \frac{8[(-1+\beta^3)(2+7\beta^3+(2+\beta^3)\sqrt{1+8\beta^3})]}{9[\sqrt{1+8\beta^3}(3+\sqrt{1+8\beta^3})^2]}u^3. \tag{A8}$$

To the lowest order in u, the values of $\mathrm{Im}\,(\Lambda)$ for each mode are given by

$$\lim_{u\to 0}\,[\mathrm{Im}\,(\Lambda_1)] = \frac{4(-1+\beta^3)}{3(-3+\sqrt{1+8\beta^3})} = \frac{1}{2}+\frac{1}{6}\sqrt{1+8\beta^3}, \tag{A9}$$

$$\lim_{u\to 0}[\mathrm{Im}(\Lambda_2)] = -\frac{4(-1+\beta^3)}{3(+3+\sqrt{1+8\beta^3})} = \frac{1}{2}-\frac{1}{6}\sqrt{1+8\beta^3}, \tag{A10}$$

while those of $\mathrm{Re}\,(\Lambda)$ are given by

$$\lim_{u\to 0}[\mathrm{Re}(\Lambda_1)] = -\frac{8\{(-1+\beta^3)[-2-7\beta^3+(2+\beta^3)\sqrt{1+8\beta^3}]\}}{9[\sqrt{1+8\beta^3}(-3+\sqrt{1+8\beta^3})^2]}u^3 = \frac{1}{9}(1-\beta^3)\left(1-\frac{1}{\sqrt{1+8\beta^3}}\right)u^3, \tag{A11}$$

$$\lim_{u\to 0}[\mathrm{Re}(\Lambda_2)] = \frac{8[(-1+\beta^3)(2+7\beta^3+(2+\beta^3)\sqrt{1+8\beta^3})]}{9[\sqrt{1+8\beta^3}(3+\sqrt{1+8\beta^3})^2]}u^3 = \frac{1}{9}(1-\beta^3)\left(1+\frac{1}{\sqrt{1+8\beta^3}}\right)u^3. \tag{A12}$$

These analytic expressions reproduce Figs. 2(a) and 2(b) so closely that the difference is invisible. [For comparison purposes, recall that $\Lambda_D = \frac{2}{9}(1-\beta^3)u^3$.]

[1] R. H. Dicke, Phys. Rev. **93**, 99 (1954).
[2] V. M. Fain, Sov. Phys. JETP **36**, 798 (1959).
[3] N. E. Rehler and J. H. Eberly, Phys. Lett. A **29**, 142 (1969); Phys. Rev. A **3**, 1735 (1971).
[4] J. Mostowski and B. Sobolewska, Phys. Rev. A **28**, 2943 (1983).
[5] S. Prasad and R. J. Glauber, Phys. Rev A **31**, 1583 (1985).
[6] M. O. Scully, E. S. Fry, C. H. R. Ooi, and K. Wódkiewicz, Phys. Rev. Lett. **96**, 010501 (2006); I. E. Mazets and G. Kurizki, J. Phys. B **40**, F105 (2007).
[7] R. Friedberg, S. R. Hartmann, and J. T. Manassah, Phys. Lett. A **40**, 365 (1972).
[8] R. Friedberg and S. R. Hartmann, Opt. Commun. **10**, 298 (1974); Phys. Rev. A **10**, 1728 (1974).
[9] S. Prasad and R. J. Glauber, Phys. Rev. A **82**, 063805 (2010).
[10] R. Friedberg and J. T. Manassah, Phys. Lett. A **372**, 6833 (2008).
[11] R. Friedberg and J. T. Manassah, Phys. Lett. A **373**, 4416 (2009).
[12] R. Friedberg, S. R. Hartmann, and J. T. Manassah, Phys. Rep. **7**, 101 (1973); J. T. Manassah, *ibid.* **101**, 359 (1983).
[13] V. A. Sautenkov, Laser Phys. Lett. **8**, 771 (2011).
[14] R. Bonifacio, P. Schwendimann, and F. Haake, Phys. Rev. A **4**, 302 (1971).
[15] R. Friedberg and J. T. Manassah, Opt. Commun. **282**, 3089 (2009).
[16] J. T. Manassah, Phys. Rev. A **82**, 053816 (2010).